Raman Spectroscopy Measurements of the Pressure–Temperature Behavior of LiAlH 4

ARTICLE *in* THE JOURNAL OF PHYSICAL CHEMISTRY C · JULY 2010

Impact Factor: 4.77 · DOI: 10.1021/jp1015017

Raman Spectroscopy Measurements of the Pressure−Temperature Behavior of $LiAlH_4$

Juan C. Fallas, Wen-Ming Chien, Dhanesh Chandra,* and Vamsi K. Kamisetty

Materials Science and Engineering Division, Department of Chemical and Metallurgical Engineering (MS 388), University of Nevada, Reno, Reno, Nevada 89557

Erik D. Emmons

U.S. Army Edgewood Chemical Biological Center, AMSRD-ECB-RT-DL/BLDG E5560, 5183 Blackhawk Road, Aberdeen Proving Ground, Maryland 21010-5424

Aaron M. Covington

Department of Physics and Nevada Terawatt Facility (MS 220), University of Nevada, Reno, Reno, Nevada 89557

Raja Chellappa, Stephen A. Gramsch, and Russell J. Hemley

Geophysical Laboratory, Carnegie Institution of Washington, 5251 Broad Branch Road NW, Washington, D.C. 20015

Hans Hagemann

Department of Physical Chemistry, University of Geneva, 30 Quai Ernest Ansermet, CH-1211, Geneva, Switzerland

Received: February 18, 2010; Revised Manuscript Received: June 1, 2010

The pressure/temperature phase diagram of $LiAlH_4$ has been constructed by using Raman spectroscopy data. In situ high pressure−temperature experiments were carried out using resistively heated diamond anvil cells up to 150 °C and 7 GPa. Room temperature phase transitions of monoclinic α-$LiAlH_4$ → δ-$LiAlH_4$ were observed at ∼3.2 GPa. As the temperature is increased to ∼100 °C, both the α and δ phases transform to β-$LiAlH_4$ and remain stable up to 5.5 GPa. At temperatures greater than 300 °C, a new γ-$LiAlH_4$ phase forms. Data of Konovalov (1995) has been used to define the phase boundary between β- and γ-$LiAlH_4$ phases. We present a pressure−temperature phase diagram of $LiAlH_4$ based using diamond anvil cells coupled with Raman spectroscopy.

I. Introduction

Complex alkali alumino-hydrides, such as $NaAlH_4$ and $LiAlH_4$, with ∼10.5 wt % H are potential candidates for hydrogen storage applications.[1] The dehydrogenation characteristics of $MAlH_4$ (M = Na, Li)[2] are given by

$$3MAlH_4 \rightarrow M_3AlH_6 + 2Al + 3H_2 \quad (1)$$

$$M_3AlH_6 \rightarrow 3MH + Al + \frac{3}{2}H_2 \quad (2)$$

Bogdanovic et al.[3] demonstrated that the addition of Ti-based catalysts to $NaAlH_4$ improves the compound chemical kinetics while decreasing its decomposition temperature. However, the current reversible amount of hydrogen in $NaAlH_4$ is 5.6 wt % H in the presence of a Ti-based catalyst,[4] with more work in progress.[5] The mechanochemical addition of catalysts via ball milling has been shown to be beneficial for enhancing hydrogen release kinetics. During ball milling, the hydrides can undergo local stress-induced transformations[1,6] as well as catalytic interactions. In a systematic study, Andreasen et al.[7] concluded that ball-milled $LiAlH_4$ has faster dehydrogenation kinetics than unmilled material and identified a proportional relation between milling time and the rate of dehydrogenation. A fundamental understanding of the effects of stress during ball milling is necessary to improve the process of hydrogenation mechanisms. Thus high pressure studies were undertaken in our studies prompted by the ab initio studies of Vajeeston et al.[8] who predicted α-$LiAlH_4$ → δ-$LiAlH_4$ structural transition at room temperature at 2.6 GPa with a 17% volume collapse. They[8] attributed this volume collapse due to electronic transition from *s* to *p* states of Al and much larger when compared to $NaAlH_4$ (4%). Talyzin et al.[4] reported a reversible structural phase transition from α'-$NaAlH_4$ to β-$NaAlH_4$ between 14−15 GPa. These pressure-induced transitions were confirmed by Raman spectroscopy[1] and a disorder−order transition to δ-$LiAlH_4$ at ∼3 GPa. The structure of the high pressure phase has been determined[9] to be *I*2/*b* with a large reduction in unit cell volume (26.9% at 7.15 GPa) compared to ambient pressure. Hauback[10] showed that $LiAlH_4$ presents similar characteristics in the crystalline structure of other complex aluminum based hydrides, noting that the Al−D distances are comparable in the tetrahedra and octahedra. Sundqvist and Andersson[11] mapped the *P*−*T*

* To whom correspondence should be addressed. E-mail: dchandra@unr.edu.

10.1021/jp1015017
Published on Web 06/17/2010

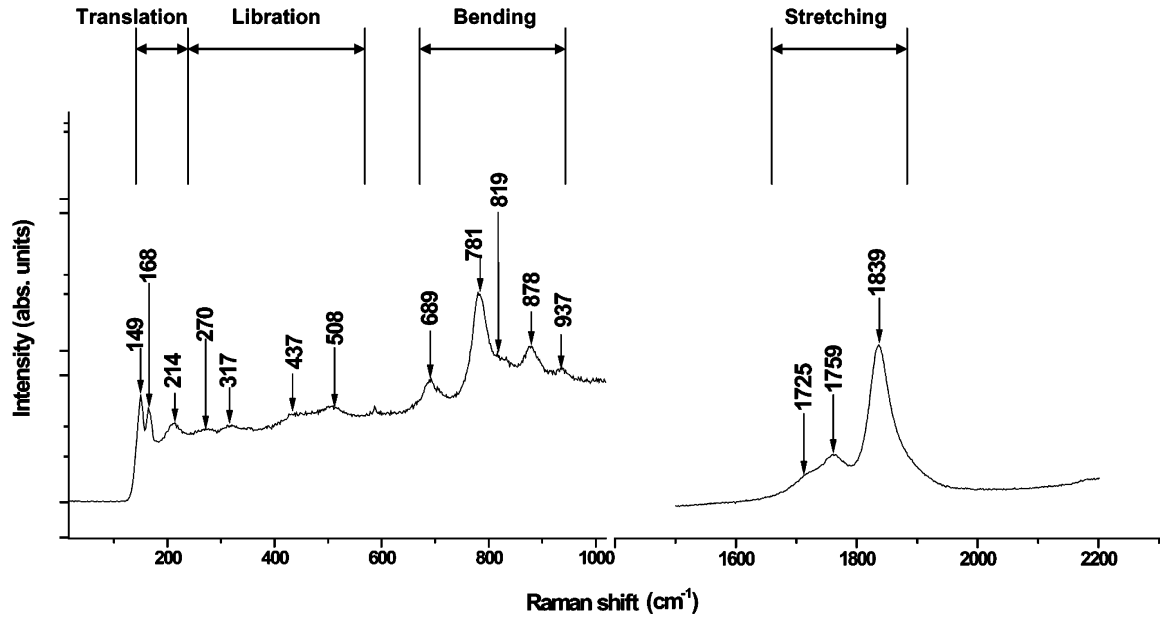

Figure 1. Mode assignments for $LiAlH_4$ from this study (as-loaded sample, ~0 GPa), showing the various vibrational modes. Peak assignments are given in Table 1.

structural phase diagram of $NaBH_4$ using thermal measurements and their results show with the tetragonal to cubic transition of $NaBH_4$ in the $P-T$ phase diagram (up to ~2 GPa and ~250 °C). A temperature-dependent Raman spectroscopy study on $NaAlH_4$ revealed possible catalytic interaction of Ti with the AlH_4^- anion, leading to a weakening of the Al−H bond strength, and disintegration of the structural unit.[12] Going back to $LiAlH_4$, Majzoub et al.[5] reported decomposition of $LiAlH_4$ above 145 °C decomposed to according to reaction 1 from Raman spectroscopy[5] measurements. Majzoub et al.[5] were unable to observe any vibrational bands in the Raman spectrum at 145 °C, although the presence of Li_3AlH_6 should have been detectable. The presence of micro or nanocrystalline aluminum may have led to excessive Rayleigh scattering, making it difficult to observe the Raman spectra, as commented in that study. $LiAlH_4$ must be handled in an inert atmosphere to avoid its decomposition. Ke et al.[13] demonstrated that $LiAlH_4$ decomposes at all temperatures and pressures studied by a computational simulation method. Mal'tseva et al.[14] emphasized that it is important to take this decomposition into account in these $LiAlH_4$ studies and demonstrated that the sample decomposed into a mixture of hydrides ambient pressure and temperature. They[14] showed that white powder of $LiAlH_4$ turned gray upon formation of metallic aluminum, which demonstrating the decomposition of the sample. As mentioned earlier, there have been some prior studies on pressure-induced transitions at room temperature on $LiAlH_4$; however, there are few reports on combined $P-T$ behavior. Bulychev et al.[15] reported a phase transition at ~7 GPa and 250−300 °C from β (tetragonal) to γ (orthorhombic)-$LiAlH_4$; and they also found β- and γ-$LiAlH_4$ phases present under ambient conditions. In addition, this author observed a change in the coordination number of Al^{3+} ion from 4 to 6 when the phase transition occurs. In our study, we have extended the phase diagram of $LiAlH_4$ studies from 22 to 150 °C and up to 7 GPa using in situ Raman spectra measurements. The pressure effects on AlH_4 unit are discussed in the various phase fields at higher temperatures.

II. Experimental Methods

The samples of $LiAlH_4$ (95% purity) were procured from Alfa Aesar and were used without any further purification process. Sample preparation was performed in a glovebox to avoid the reaction of the material with moisture and oxygen. Also, the diamond anvil cell was loaded in an inert atmosphere to prevent the same reaction possibility. Raman spectroscopy experiments were performed in the Optical Properties of Materials Laboratory in the Physics Department at the University of Nevada, Reno. The Raman spectral data were obtained with a Renishaw InVia Raman microspectroscopy system with a 20× objective lens and 514.5 nm laser using 5−10 mW of laser power incident upon the DAC. Further details of the diamond anvil cell and Raman spectrometer are available in Emmons et al.[16,17] The Raman scattering wavelength was calibrated using Ne lines, and a small offset correction was performed.[18] The $LiAlH_4$ sample in the DAC was heated with an Omega temperature controller system attached to an adjustable resistive heater. The DAC used had diamonds with 600 μm culets, and samples were loaded in a ~200 μm diameter hole in an Inconel gasket with no pressure media. Due to the reactivity of the sample, the commonly used 4:1 methanol/ethanol pressure media was not used in this study. The ruby fluorescence method[19] was used to determine the pressure inside the DAC (Cr^{3+}-doped Al_2O_3, R1 line at 694.2 nm under ambient conditions). Because the sample was heated, it is important to take into account a temperature correction in the measurement of the pressure in the DAC by the ruby fluorescence technique. Vos and Schouten[20] found an increase in the ruby wavelengths with increasing temperature at a rate of 0.0068 nm/K. Several ruby chips were distributed within the sample for the pressure measurements. The DAC was loaded and closed with minimal pressure. Because of the absence of a pressure medium, the effect of nonhydrostaticity needed to be considered. However, observation of the ruby R1 and R2 lines showed that they were well resolved, indicating a reasonably hydrostatic environment was maintained during all measurements.

III. Results

Raman Spectroscopy Results. The Raman spectrum of $LiAlH_4$ at ~0 GPa and room temperature is shown in Figure 1. The assignment of the various modes is given in Table 1 and is in good agreement with literature.[1] The spectrum is dominated by the internal modes (bending and stretching) due to Al−H bonds. The relatively high frequency indicates that the AlH_4^-

TABLE 1: Comparisons of the Vibrational Modes Assignment of $LiAlH_4$ from Experimental Raman Data

DAC as-loaded (this work)	DAC as-loaded (Chellappa et al.)[1]	powder Raman (Bureau et al.)[23]	vibrational mode assignments
	88	95	translation
	102	112	
149	141	143	
168	157	151	
214	201	165	
270	225	220	librational
317	312	322	
437	434	438	
508	495	510	
689	688	690	$\delta(AlH_2)$
781	778	780	sym-$\delta(AlH_2)$
819	816	830	$\delta(AlH_2)$
878	878	882	$\delta(AlH_2)$
937	933	950	$\delta(AlH_2)$
1725	1720	1722	ν (Al−H)
1759	1754	1762	asym-ν (Al−H)
1839	1829	1837	sym-ν (Al−H)

is a stable ion fixed in the lattice. Gorbunov et al.[21] also found a librational mode for $LiAlH_4$ at 472 cm^{-1}. The pressure- and temperature-induced changes to the $[AlH_4]^-$ unit provides information on the strength of Al−H bonding and is useful to understand hydrogen release mechanisms.

A good reference for the librational motion in $LiAlH_4$ is the study of Temme and Waddington.[22] The frequency shifts indicate that the temperature increase in the system at constant pressure is producing a phase transition from α-$LiAlH_4$ to δ-$LiAlH_4$. A shifting in the band corresponding to the stretching mode is probably the most significant difference in both Figures 1 and 2, moving from 1839 to 1749 cm^{-1}. The disappearance of the bands at 1725 and 1759 cm^{-1} at high pressure in the Al−H bond is transcendental to considerate a new molecular structure in the sample due a phase transition. Other changes in the vibrational modes and peaks at high pressure are perceptible in the bending region, having prominent peaks at 1124 and 1154 cm^{-1}, with minor bands at 911, 778, and 715 cm^{-1}. A shifting in the peaks of the librational mode is observed at ∼6.6 GPa, with bands of moderated intensity at 336, 387, 478, and 514 cm^{-1}. Finally, the translation mode has regular peaks also at higher frequencies than the data obtained at room temperature and pressure.

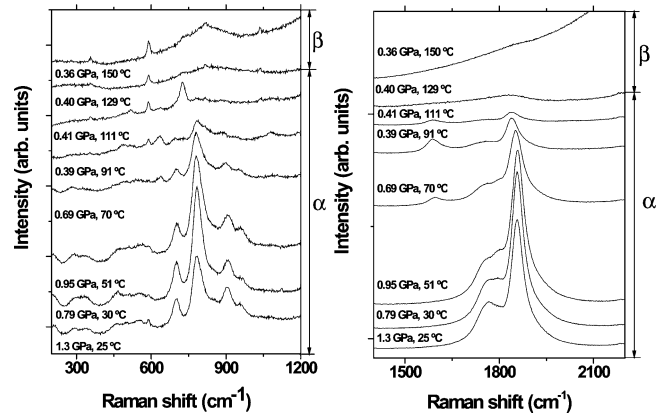

Figure 3. Temperature-dependent Raman spectra for $LiAlH_4$. By increasing the temperature of the sample at an initial pressure of ∼1.3 GPa, reorganization in the structure of the material from α to β phase was observed at 129 °C.

In this case, two peaks at 222 and 252 cm^{-1} are present in this zone of the spectra. There is no evidence or studies involving high pressure or temperature assignment of vibrational modes in $LiAlH_4$.

Pressure−Temperature Behavior of $LiAlH_4$. A series of spectra was collected in temperature increments of ∼20 °C up to 150 °C at high pressures. A heating run beginning at 1.3 GPa is shown in Figure 3. A strong band is present at ∼800 cm^{-1}, gradually reducing its intensity until its disappearance at ∼129 °C. A similar effect occurs with the adjacent bands at 700 and 900 cm^{-1} (bending vibrational modes). At ∼1850 cm^{-1}, a dramatic reduction of the intensity in the Al−H vibron is detected, decreasing completely at 129 °C. The peak at 1750 cm^{-1} looses completely its intensity at 111 °C. This effect marks the transition from α to β phases in $LiAlH_4$. Above 91 °C there

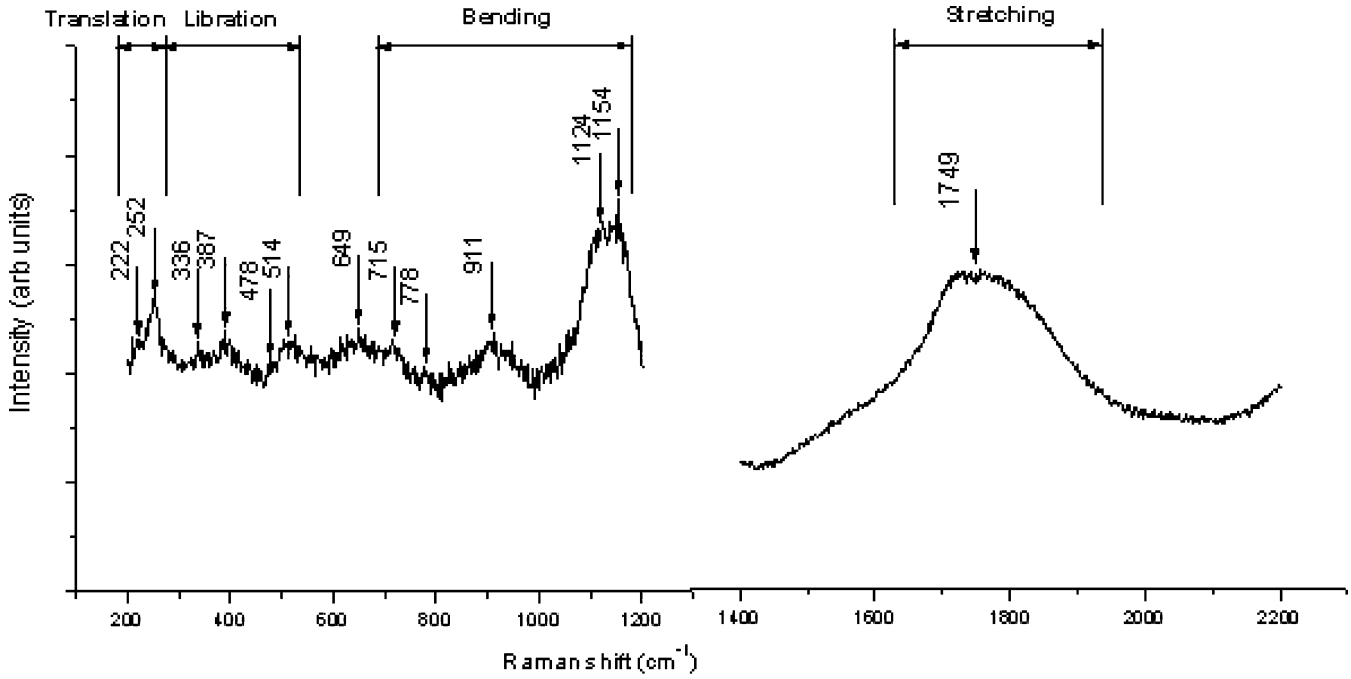

Figure 2. Mode assignments for $LiAlH_4$ from this study (as-loaded sample, ∼6.6 GPa), showing the various vibrational modes.

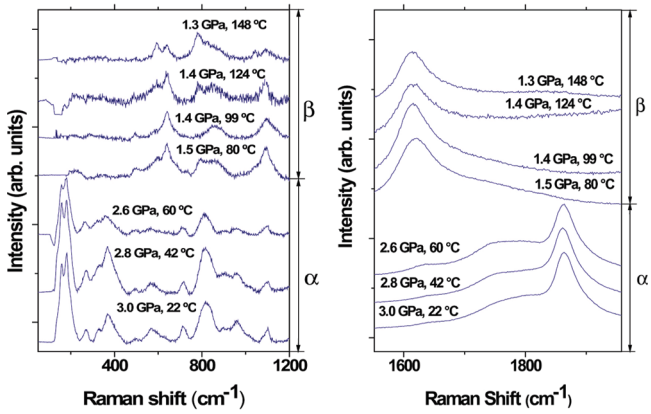

Figure 4. Temperature-dependent Raman spectra for $LiAlH_4$. By increasing the temperature of a sample initially pressurized to ~3.0 GPa, a phase transition from α to β can be observed between 60 and 80 °C.

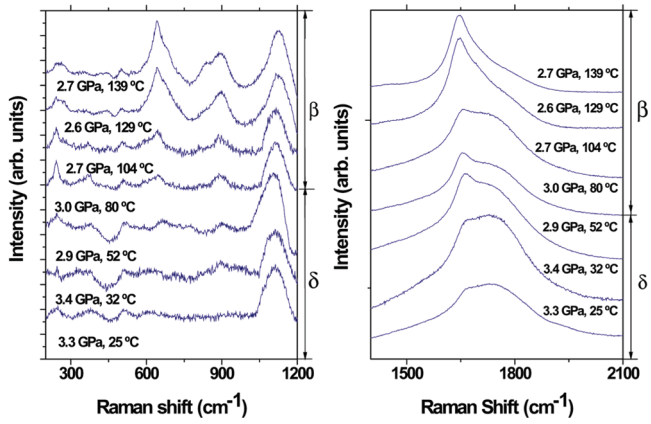

Figure 5. Temperature-dependent Raman spectra for $LiAlH_4$. By increasing the temperature of the sample at an initial pressure of ~3.3 GPa, a phase transition from δ- to β-$LiAlH_4$ can be observed between 104 and 129 °C.

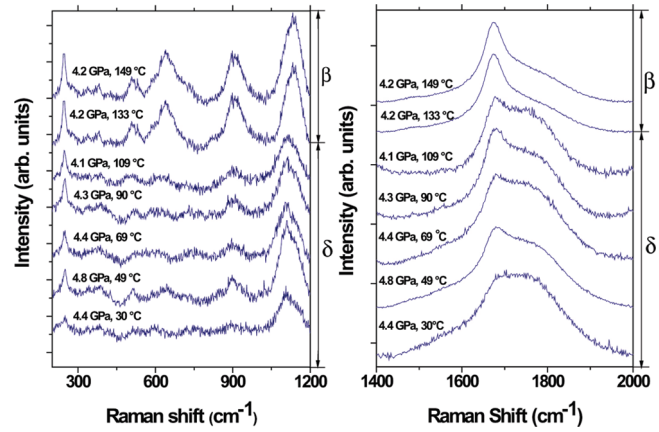

Figure 6. Temperature-dependent Raman spectra for $LiAlH_4$. By increasing the temperature of the sample at initial pressure of ~4.4 GPa, a phase transition from δ- to β-$LiAlH_4$ can be observed between 109−133 °C.

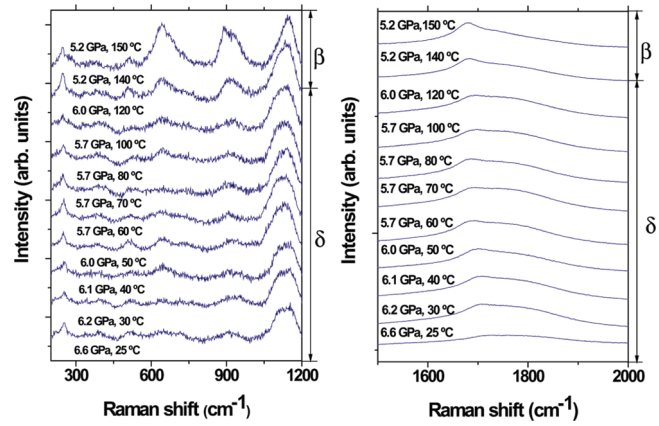

Figure 7. Temperature-dependent Raman spectra for $LiAlH_4$. By increasing the temperature of the sample at an initial pressure of ~6.6 GPa, a phase transition from δ- to β-$LiAlH_4$ can be observed between 120−140 °C.

are signals of the phase transition zone, with new peaks at ~600 and ~650 cm^{-1}, surviving only the first one in the new phase. Above 70 °C, similar behavior can be observed in the high frequency region, specifically at ~1600 cm^{-1}.

In Figure 4, pressure was initially set near 3 GPa at room temperature, to be slightly below the pressure-induced orientational-disorder phase transition of $LiAlH_4$. Significant changes are seen between 60−80 °C with a drop in pressure from 2.6 to 1.5 GPa. At 3 GPa, between 60 and 80 °C, Al−H bands at 1850 cm^{-1} disappear completely. The new band at 1600 cm^{-1} is seen up to 147 °C without broadening. At 3.0 GPa, a band at 1100 cm^{-1} already present at 22 °C undergoes significant changes between 60 and 80 °C, with further changes between 124 and 148 °C. In the lower frequency region, there is a loss of crystallinity with the disappearance of the lattice modes.

An increase of the intensity in the peak is seen at ~1100 cm^{-1} starting at the phase transition temperature (~60 °C). Additionally, the formation of new bands at ~650 cm^{-1} provides substantial evidence of the phase transition in the material. Softening in the intensity of the strong peak at ~800 cm^{-1} was observed and the shoulders present at 700 and 900 cm^{-1}. The Raman spectra at an initial pressure of ~3.3 GPa showed evidence for structural changes in the material upon heating (Figure 5); this pressure was selected to be just above the orientational disorder transition pressure. The Al−H stretching modes show clear evidence of the transition, with a softening above the transition temperature and a sharpening of the main feature in this region.

Between 104 and 129 °C, disappearance of the 1780 cm^{-1} band occurs, along with the appearance of new bands at 650, 900, and 1120 cm^{-1}, being characteristic of β phase as will be explained. We designed the experiments by intentionally selecting the pressure values slightly below and above the $\alpha \Leftrightarrow \delta$ phase transition in $LiAlH_4$, starting from the δ phase of the material under study (in Figure 5). Increasing the temperature initially leads to a slight pressure drop due the DAC and its relaxation brought a combination of factors. When the temperature was raised from 32 to 52 °C, the pressure dropped from 3.4 to 2.9 GPa still maintaining δ phase (Figure 5). Also, the δ phase is stable at higher pressures, 4.4 GPa (Figure 6) and 6.6 GPa (Figure 7). Probably the best point of reference is the strong band that exists at ~1100 cm^{-1} (bending mode zone), which is common for the figures with δ-$LiAlH_4$ Raman spectra. Other features such as those present at ~650 and ~250 cm^{-1} are characteristics in that specific phase. Apart, the peaks detected in the β region of Figure 4 share similarities with the obtained in the β zone of Figure 5, as well as the bands detected in further experiments (~1100, ~650, and ~900 cm^{-1}). The heating run starting from δ-$LiAlH_4$ phase at 4.4 (30 °C) and 6.2 GPa are shown in Figures 6 and 7 with changes occurring 109−133 °C and 120−140 °C, respectively.

Both Figures 5 and 6 share features because they are having a similar δ- to β-$LiAlH_4$ transition, such as the prominent peak at ~1100 cm^{-1}, which increase its intensity when the phase transition happen. The peaks present at ~650, ~250, and ~900 cm^{-1} are also common in Figures 6 and 7. The β-$LiAlH_4$ characteristic bands explained for the case of Figures 4 and 5 are present in the data obtained for the specific experiments under study. The Al−H bond behavior is notorious in Figure 6, where at 109 °C the band present at ~1700 cm^{-1} increases its sharpness due the reach of the phase transition temperature. Nevertheless, Figure 7 shows an evolution on the stretching bond, while the temperature is increased. At 120 °C, when the phase transition occurs, it is possible to see how the band becomes sharp.

IV. Discussion

Hydrogen release in aluminohydrides must involve the breaking of the strong covalent Al−H bond in the $[AlH_4]^-$ unit.[25,26] It is interesting to note that at room temperature there is a pressure-induced weakening of Al−H bonds in $LiAlH_4$[8,9,27] as well as B−H bonds in $NaBH_4$[11,28] and $LiBH_4$[29] resulting in disorder in the high pressure phases. There is a parallel to the pressure and temperature effects on AlH_4 unit[5] and in case of $NaAlH_4$ that Al−H stretching and bending modes do not weaken noticeably with pressure remaining stable even in the melt. As mentioned earlier, the action of Ti-based catalysts may be to facilitate the weakening of the AlH_4 tetrahedra. It is informative to compare the experimental results shown in Figures 4 and 5. The main difference observed is that the pressure drop due to temperature increases in Figure 5 is not as large as that observed in Figure 4, resulting in a more constant pressure in the experiment. The shifting of the bands in Figure 4 presents a clear transition. Although the shifting of the features in Figure 5 is not as remarkable as in Figure 4, the δ-$LiAlH_4$ to β-$LiAlH_4$ phase transition between 104 and 129 °C can be observed. There were also significant changes in the Al−H stretching modes at higher temperatures. At low temperatures in the orientationally disordered phase (Figures 5−7), there is a broad Al−H stretching feature present in the vicinity of 1700 cm^{-1}. As the sample is heated, a sharper feature, in the range from 1630−1680 cm^{-1}, becomes superimposed upon the broad peak. These changes are correlated with the changes in the Al−H bending modes and indicate significant structural changes in the sample. The sharper profile of the features may indicate a decrease in the level of disorder. Another valuable experimental publication related to the present study was performed by Pitt et al.[9] using neutron diffraction to characterize the crystalline structure of $LiAlD_4$ at high pressure. Their research determined that there is a coexistence of phases at 60 °C and 7.15 GPa, α-$LiAlD_4$ has lattice parameters of $a = 4.328(2)$ Å, $b = 6.715(2)$ Å, $c = 7.231(3)$ Å, and $\beta = 105.29(5)°$, with a space group of $P2_1/c$ and δ-phase of $LiAlD_4$ is monoclinic (I_2/b), and its lattice parameters are $a = 4.099(3)$ Å, $b = 4.321(4)$ Å, $c = 10.006(3)$ Å, and $\gamma = 88.43(4)°$, being consistent with a distorted AlH_4^- tetrahedron. They also found a reversible phase transition (from β to α phase) when the sample underwent a slow pressure release and was then cooled from a temperatures of 60 °C. At 295 K, Hauback et al.[30] performed a study on $LiAlD_4$ by neutron diffraction and powder X-ray diffraction. A trigonal bipyramid of five deuterium atoms from five neighboring $[AlD_4]^-$ tetrahedral surrounds the Li atoms. At 295 K, $LiAlD_4$ has lattice parameters of $a = 4.83(1)$, $b = 7.80(1)$, and $c = 7.90(1)$ Å. At low temperatures, there is an increase in a minor distortion of the AlD tetrahedra. Also, the experiments determined that the

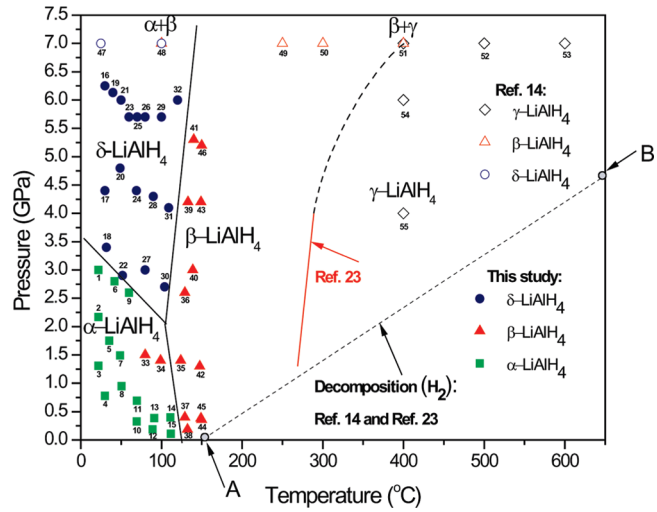

Figure 8. Experimental pressure−temperature phase diagram of $LiAlH_4$. The diagram is based on the variable pressure and temperature measurements. To enhance the phase diagram we used data from refs 14 and 23 in our $P-T$ diagram.

distances of the Al−D bond are in the range of 1.60(7)−1.63(5) Å at 295 K and 1.60(6)−1.65(5) Å at 8 K. In an early study of $LiAlH_4$, Bulychev et al.[15] also made reference to the crystal structure properties of this material and its phases. In their quenched samples, the α-phase (δ in our nomenclature) is given as monoclinic, with a calculated density of 0.917 g/cm^3 and unit cell parameters of $a = 9.6$ Å, $b = 7.86$ Å, $c = 7.90$ Å, and $z = 4$. The structure of β-$LiAlH_4$ is tetragonal, with lattice parameters of $a = 6.75$ Å, $c = 8.081$ Å, $z = 6$, and a calculated density of 1.02 g/cm^3. Finally, the γ-phase is orthorhombic, with lattice parameters of $a = 5.11$ Å, $b = 9.21$ Å, $c = 4.29$ Å, and $z = 4$. The γ-$LiAlH_4$ density was calculated to be 1.20 g/cm^3. Talyzin and Sundquist[27] reported that the crystal structure in the high pressure α-$LiAlH_4$ phase is not the same as that of α-$NaAlH_4$ after observing a triplet structure for the Al−H stretching modes in high pressure β-$LiAlH_4$. This conclusion is based upon the observation of two strong peaks in the Raman spectra of $LiAlH_4$, in the Al−H stretching region, and is in contrast with the results of Chellappa et al.[1] It is not obvious to draw a clear correlation between Al−H bond lengths in $LiAlH_4$ measured by neutron powder diffraction for the alpha and delta phases (Pitt et al.[9]) and the Al−H stretching mode seen by Raman spectroscopy. Indeed, the Al−H Raman stretching modes at room temperature shift significantly to lower frequencies with increasing pressure at the alpha-delta phase transition (around 3 GPa) except for one weak band, while the Al−D bond length becomes shorter. This conflicts with the correlation reported by Yukawa et al.[31] for the sodium alanates; thus, this discrepancy exists. If this correlation is generally applicable, it implies that for $LiAlH_4$ the Al−H bonds become longer at higher pressures, which must then be associated with an increase of the coordination number (for example, from 4 to 6) for the central Al atom. This is in principle possible, but it is not confirmed by the neutron powder diffraction data by Pitt et al.[9] Another potential explanation for this shift to lower frequencies may arise from a change of the bonding properties, that is, the Li−H bonds become stronger and the Al−H bonds become weaker upon compression. Note that the Raman stretching bands observed in this study are rather broad, which does not help to monitor the changes and also suggests either dynamical behavior or disorder in the structure.

$LiAlH_4$ $P-T$ Phase Diagram. Based on the changes of the vibrational modes discussed previously, along with the literature

TABLE 2: Summary Table of $LiAlH_4$ ($LiAlD_4$) from Literature Results[a]

data in Figure *8*	ref	compound	experimental conditions	space group	*a* (Å)	*b* (Å)	*c* (Å)	β/γ (deg)	Al−H/Al−D bond length (Å)
	Hauback et al. (2002)[30]	α-$LiAlD_4$	295 K	$P2_1/c$	4.8254(1)	7.8040(1)	7.8968(1)	$\beta = 112.268(1)$	1.603(7)−1.633(5)
	Pitt et al. (2005)[9]	α-$LiAlD_4$	293 K, 3.25 GPa	$P2_1/c$	4.563(3)	6.833(4)	7.692(5)	$\beta = 110.57(7)$	1.559(2)−1.725(2)
48, 49, 50, 51	Bulychev et al. (1977)[15]	β-$LiAlH_4$	523 − 573 K, 7 GPa		6.75		8.081		
47, 48	Bulychev et al. (1977)[15]	δ-$LiAlH_4$	298 K, 7 GPa	$P2_1/c$	9.6	7.86	7.90	$\beta = 121$	1.55
	Pitt et al. (2005)[9]	δ-$LiAlD_4$	333 K, 7.15 GPa	$I2/b$	4.099(3)	4.321(2)	10.006(3)	$\gamma = 88.43(4)$	1.545(2)
51, 52, 53	Bulychev et al. (1977)[15]	γ-$LiAlH_4$	773 K, 7 GPa	*Pnma*	5.11	9.21	4.29		
	Hauback et al. (2003)[33]	$NaAlD_4$	295 K	$I4_1/a$	5.0119(1)		11.3147(5)		1.627(2)
	Kumar et al. (2007)[34]	$NaAlH_4$	295 K	$I4_1/a$	5.0019(1)		11.298(1)		
	Hauback et al. (2005)[35]	$KAlH_4$	295 K	*Pnma*	8.8515(14)	5.8119(8)	7.3457(11)		1.618
	Bastide et al. (1995)[36]	$RbAlH_4$		*Pnma*	9.253	5.950	7.599		
	Bastide et al. (1995)[36]	$CsAlH_4$		*Pnma*	9.981	6.075	7.953		

[a] Note: Points 48 and 51 in Figure 8 (*PT* phase diagram of $LiAlH_4$) are included in two different phases in this table, because Bulychev's paper shows a mixing of phases.

data, the *P*−*T* phase diagram of $LiAlH_4$ is established, as shown in Figure 8. The transition from α to β is sluggish, with a possibility of an α+β mixed phase between 80−100 °C and ∼1.5 GPa. A dramatic weakening of the Al−H bond is seen in Figure 4 from 60 to 90 °C. In the phase transition from α-$LiAlH_4$ to β-$LiAlH_4$, it is also remarkable that the Raman spectrum of this phase presents similar features compared to a sample of $NaAlH_4$ cooled from 508 K to room temperature, which have been assigned to AlH_6 vibrations by analogy with reported data for Na_3AlH_6 (Bureau). The γ phase is characterized by very broad bands at 1750 and 1100 cm^{-1}. The band at 1650 cm^{-1} could in fact originate from α phase, with a transition temperature increasing with pressure. Note that this phase does not show the expected AlH_4 bending modes around 750 and 900 cm^{-1}. The transition among the phases β and γ in the *PT* phase diagram was observed in the experiments of Konovalov et al.,[24] who plotted a line in the phase from approximately 250−350 °C and 0.5−7.5 GPa. The line is shown in the phase diagram below. Bulychev et al.[15] also detected phase transitions in the *PT* phase diagram of $LiAlH_4$ in their quenched samples. At a constant pressure of approximately 7 GPa, they were able to observe a phase transition in the material from δ-$LiAlH_4$ to γ-$LiAlH_4$ at 400 °C. The transition matches with the Konovalov et al.[24] study, and examine regions of the *PT* phase diagram above the maximum temperature used in the present study. Finally, the decomposition line was approximated using data of Block and Gray[32] establishing one point (A) at atmospheric pressure and 150 °C decomposition temperature. We performed a linear extrapolation of the decomposition line using Bulychev et al.[15] data at a higher pressure point (B), at 7 GPa and 900 °C. A summary table of $LiAlH_4$ ($LiAlD_4$) from this study and others' results are listed in Table 2.

V. Conclusions

A *P*−*T* phase diagram of $LiAlH_4$ has been determined from 0−6 GPa and 25−150 °C using in situ Raman spectroscopy. The room temperature phase transition from ambient pressure α-$LiAlH_4$ to δ-$LiAlH_4$ was observed at ∼3.0 GPa, in agreement with literature. In the high frequency region of the Raman spectra it is possible to see a significant change in the peaks of the Al−H stretching modes, corresponding to the phase transitions in each case. X-ray diffraction measurements are required to resolve the nature of the phases in $LiAlH_4$ and can also provide a better understanding of volume collapse phenomena in the material.

Acknowledgment. We thank our DOE funding agency for the support of the program (CDAC: DE-FC-03-03NA00144). We gratefully acknowledge the support of Carnegie Institution of Washington. We also thank the Optical Properties of Materials Laboratory, UNR, and gratefully acknowledge support from the US DOE under Grant No. DEFC52-06NA27616. J.C.F. acknowledges the Costa Rican National Council of Science and Technology (CONICIT).

Supporting Information Available: Symmetry analysis for $LiAlH_4$. Tables 3−5 summarize previous experimental results and define the nomenclature used in this study for the different phases encountered for $LiAlH_4$ This material is available free of charge via the Internet at http://pubs.acs.org.

References and Notes

(1) Chellappa, R. S.; Chandra, D.; Gramsch, S. A.; Hemley, R. J.; Lin, J. F.; Song, Y. *J. Phys. Chem. B* **2006**, *110*, 11088.
(2) Dymova, T. N.; Aleksandrov, D. P.; Konoplev, V. N.; Silina, T. A.; Sizareva, A. S. *Koordinatsionnaya Khimiya* **1994**, *20*, 279.
(3) Bogdanovic, B.; Schwickardi, M. *J. Alloys Compd.* **1997**, *253*, 1.
(4) Talyzin, A. V.; Sundqvist, B. *High Pressure Res.* **2006**, *26*, 165.
(5) Majzoub, E.; Ronnebro, E.; Seballos, L.; Newhouse, R.; Zhang, J. Z. *Sol. Hydrogen Nanotechnol. II* **2007**, 6650.
(6) Balema, V. P.; Pecharsky, V. K.; Dennis, K. W. *J. Alloys Compd.* **2000**, *313*, 69.
(7) Andreasen, A.; Vegge, T.; Pedersen, A. S. *J. Solid State Chem.* **2005**, *178*, 3672.
(8) Vajeeston, P.; Ravindran, P.; Vidya, R.; Fjellvag, H.; Kjekshus, A. *Phys. Rev. B* **2003**, 68.
(9) Pitt, M. P.; Blanchard, D.; Hauback, B. C.; Fjellvag, H.; Marshall, W. G. *Phys. Rev. B* **2005**, *72* (21), 214113/1–214113/9.
(10) Hauback, B. *Z. Kristallogr.* **2008**, 636.
(11) Sundqvist, B.; Andersson, O. *Phys. Rev. B* **2006**, 73.
(12) Majzoub, E. H.; McCarty, K. F.; Ozolins, V. *Phys. Rev. B* **2005**, *71*, 024118/1−024118/10.
(13) Ke, X.; Chen, C. F. *Phys. Rev. B* **2007**, *76*, 024112.
(14) Mal'tseva, N. N.; Golovanova, A. I. *Russ. J. Appl. Chem.* **2000**, *73*, 747.
(15) Bulychev, B. M.; Verbetskii, V. N.; Semenenko, K. N. *Russ. J. Inorg. Chem.* **1977**, *22*, 1611.
(16) Emmons, E. D.; Kraus, R. G.; Duvvuri, S. S.; Thompson, J. S.; Covington, A. M. *J. Polym. Sci., Part B: Polym. Phys.* **2007**, *45*, 358.
(17) Emmons, E. D.; Velisavljevic, N.; Schoonoiver, J. R.; Dattelbaum, D. M. *Appl. Spectrosc.* **2008**, *62*, 142.
(18) Song, Y.; Hemley, R. J.; Mao, H. K. A.; Liu, Z. X.; Herschbach, D. R. *Chem. Phys. Lett.* **2003**, *382*, 686.
(19) Gillet, P.; Hemley, R. J.; McMillan, P. F. Vibrational properties at high pressures and temperatures. In. *Ultrahigh-Press. Mineral.* **1998**, *37*, 525.
(20) Vos, W. L.; Schouten, J. A. *J. Appl. Phys.* **1991**, *69*, 6744.
(21) Gorbunov, V. E.; Gavrichev, K. S.; Sharpataya, G. A. *Zh. Neorg. Khim.* **1988**, *33*, 2678.
(22) Temme, F. P.; Waddington, T. C. *J. Chem. Soc., Faraday Trans.* **1973**, *69*, 783.
(23) Bureau, J. C.; Bonnetot, B.; Claudy, P.; Eddaoudi, H. *Mater. Res. Bull.* **1985**, *20*, 1147.
(24) Konovalov, S. K.; Bulychev, B. M. *Inorg. Chem.* **1995**, *34*, 172.
(25) Yoshino, M.; Komiya, K.; Takahashi, Y.; Shinzato, Y.; Yukawa, H.; Morinaga, M. *J. Alloys Compd.* **2005**, *404*, 185.

(26) Chellappa, R. S.; Chandra, D.; Somayazulu, M.; Gramsch, S. A.; Hemley, R. J. *J. Phys. Chem. B* **2007**, *111*, 10785.
(27) Talyzin, A. V.; Sundqvist, B. *Phys. Rev. B* **2004**, *70*, 180101/1–180101/3.
(28) Araujo, C. M.; Ahuja, R.; Talyzin, A. V.; Sundqvist, B. *Phys. Rev. B* **2005**, *72*, 054125/1−054125/5.
(29) Talyzin, A. V.; Andersson, O.; Sundqvist, B.; Kurnosov, A.; Dubrovinsky, L. *J. Solid State Chem.* **2007**, *180*, 510.
(30) Hauback, B. C.; Brinks, H. W.; Fjellvag, H. *J. Alloys Compd.* **2002**, *346* (1−2), 184–189.
(31) Yukawa, H.; Morisaku, N.; Li, Y.; Komiya, K.; Rong, R.; Shinzato, Y.; Sekine, R.; Morinaga, M. *J. Alloys Compd.* **2007**, *446−447*, 242–247.
(32) Block, J.; Gray, A. P. *Inorg. Chem.* **1965**, *4*, 304.
(33) Hauback, B. C.; Brinks, H. W.; Jensen, C. M.; Murphy, K.; Maeland, A. J. *J. Alloys Compd.* **2003**, *358*, 142–145.
(34) Kumar, R. S.; Kim, E.; Tschauner, O.; Corneluis, A. L.; Sulic, M. P.; Jensen, C. M. *Phys. Rev. B* **2007**, *75*, 174110.
(35) Hauback, B. C.; Brinks, H. W.; Heyn, R. H.; Blom, R.; Fjellvag, H. *J. Alloys Compd.* **2005**, *394*, 35–38.
(36) Bastide, J. P.; El Hajri, J.; Claudy, P.; El Hajbi, A. *Synth. React. Inorg., Met.-Org. Chem.* **1995**, *25*, 1037–1047.

JP1015017